DRAGON: Enhancing On-Device Model Performance with Distributed Retrieval-Augmented Generation

Shangyu Liu, Zhenzhe Zheng*, Xiaoyao Huang†, Fan Wu, Guihai Chen, Jie Wu†⋆
Shanghai Jiao Tong University, ⋆Temple University
†Cloud Computing Research Institute, China Telecom
{liushangyu,zhengzhenzhe}@sjtu.edu.cn, huangxy32@chinatelecom.cn,
{fwu, gchen}@cs.sjtu.edu.cn, jiewu@temple.edu

Abstract

Small language models (SLMs) support efficient deployments on resource-constrained edge devices, but their limited capacity compromises inference performance. Retrieval-augmented generation (RAG) is a promising solution to enhance model performance by integrating external databases, without requiring intensive on-device model retraining. However, large-scale public databases and user-specific private contextual documents are typically located on the cloud and the device, respectively, while existing RAG implementations are primarily centralized. To bridge this gap, we propose DRAGON, a distributed RAG framework to enhance on-device SLMs through both general and personal knowledge without the risk of leaking document privacy. Specifically, DRAGON decomposes multi-document RAG into multiple parallel token generation processes performed independently and locally on the cloud and the device, and employs a newly designed Speculative Aggregation, a dual-side speculative algorithm to avoid frequent output synchronization between the cloud and device. A new scheduling algorithm is further introduced to identify the optimal aggregation side based on real-time network conditions. Evaluations on real-world hardware testbed demonstrate a significant performance improvement of DRAGON—up to 1.9× greater gains over standalone SLM compared to the centralized RAG, substantial reduction in per-token latency, and negligible Time to First Token (TTFT) overhead.

CCS Concepts

• **Networks** → **Network services**; • **Computing methodologies** → **Distributed computing methodologies**.

Keywords

device-cloud collaborative inference, speculative aggregation, large language model, retrieval-augmented generation

This work was supported in part by National Key R&D Program of China (No. 2023YFB4502400), in part by China NSF grant No. 62322206, 62132018, 62025204, U2268204, 62272307, 62372296. The opinions, findings, conclusions, and recommendations expressed in this paper are those of the authors and do not necessarily reflect the views of the funding agencies or the government.
*Zhenzhe Zheng is the corresponding author.

MobiHoc '25, October 27–30, 2025, Houston, TX, USA

ACM ISBN 979-8-4007-1353-8/25/10
https://doi.org/10.1145/3704413.3764419

ACM Reference Format:
Shangyu Liu, Zhenzhe Zheng*, Xiaoyao Huang†, Fan Wu, Guihai Chen, Jie Wu†⋆ . 2025. DRAGON: Enhancing On-Device Model Performance with Distributed Retrieval-Augmented Generation. In *International Symposium on Theory, Algorithmic Foundations, and Protocol Design for Mobile Networks and Mobile Computing (MobiHoc '25), October 27–30, 2025, Houston, TX, USA.* ACM, New York, NY, USA, 10 pages. https://doi.org/10.1145/3704413.3764419

1 Introduction

Although large language models (LLMs) such as GPT-4 [26] and DeepSeek-V3 [9] have demonstrated remarkable performance in real-world applications, their substantial deployment costs have led to predominant cloud-based hosting. As a result, users are required to upload private context along with their queries, raising serious privacy concerns. Recently, small language models (SLMs) such as Phi-4-mini [1] and Qwen2.5-1.5B [34], have emerged as promising alternatives, offering efficient local deployment on edge devices. However, although SLMs are notably smaller than cloud-hosted LLMs—leading to reduced performance on both personal and general tasks—they still remain too large for resource-constrained devices to support on-device fine-tuning or training [16] to adapt to newly generated data and user feedback.

Retrieval-augmented generation (RAG) [21, 29] has demonstrated effectiveness in boosting the performance of SLMs by incorporating contextually relevant documents from external databases. The performance gain increases monotonically with the scale of the database, showing an opportunity for SLMs to achieve comparable or even better performance than standalone LLMs [8]. More importantly, by expanding user-specific external database (also known as the non-parametric memory [21]), model customization and knowledge updates can be achieved efficiently without model training. Typically, large-scale public databases containing general knowledge are hosted in the cloud, whereas user-specific private databases are maintained on-device. Since the query context may involve both general and personal data, it is essential for retrieval-augmented SLMs to support distributed databases located in the cloud and device. Unfortunately, most existing RAG solutions [4, 21, 29] adopted a centralized architecture. Figure 1 presents an example of game recommendation. The cloud-only RAG returns an incorrect game genre, although private documents indicate a preference for simulation games, while the device-only RAG fails to retrieve the best-selling game lists without accessing to general knowledge in the cloud.

An intuitive solution, similar to federated search [32], is to retrieve documents from the cloud-side database, merge them with those retrieved locally on-device, and perform model inference in

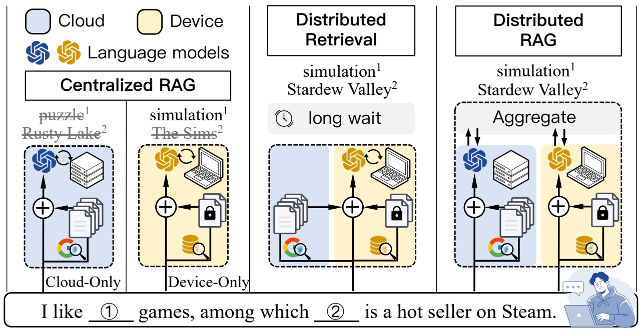

Figure 1: Comparison between different RAG architectures.

a centralized manner. However, this approach may incur substantial latency overhead considering key-value (KV) caching [42], a fundamental mechanism in language model serving that stores intermediate attention states to enable efficient reuse of past computations. The KVs of documents are typically pre-computed and persistently stored in the database to facilitate retrieval, introducing a data volume several orders of magnitude larger than the original text. This leads to a dilemma: when retrieving the raw text of cloud-side documents, the device must compute their KVs from scratch, incurring significant computation latency; Conversely, direct retrieval of KVs from the cloud storage introduces substantial transmission latency, as the data volume can be even larger than the model parameters, especially as the number of document grows.

To address these issues, we propose DRAGON, a distributed retrieval-augmented generation framework designed to enhance the performance of on-device language model inference. Following the law of total probability, DRAGON first decomposes the multi-document RAG process into a dual-side workflow by the device and the cloud, respectively, and then aggregates their output tokens for the final result. In this workflow, the cloud and device sides independently execute their own model instances using documents retrieved from their databases. Document KVs are stored and loaded locally without transmission or re-computation, thereby reducing first-token latency and preserving document privacy. Nonetheless, the output aggregation requires frequent exchange of data packets between the cloud and device at every token generation step, due to the auto-regressive nature of language models. This transmission pattern requires a persistent low-latency network connection, which is difficult to guarantee in real-world scenarios [24].

To solve this challenge, we draw inspiration from the draft-then-verify paradigm in *Speculative Decoding* [20] and propose a new dual-side speculative algorithm, namely *Speculative Aggregation*. In this algorithm, the decoding processes on both sides continuously generates draft tokens, and an Aggregator on either side (depending on certain scheduling criteria) asynchronously verifies and aggregates them. Decoding is interrupted and the corresponding KV states are rolled back for re-computation only when a draft is rejected. As our theoretical analysis proves the equivalence between Speculative Aggregation and the vanilla synchronized version, the end-to-end latency can be reduced by overlapping transmission and decoding processes.

We implement a fully-functional distributed RAG workflow and construct a testbed using real-world hardware. Based on this, we evaluate DRAGON against various RAG architectures using representative SLMs on large-scale retrieval corpora and datasets. Experimental results on language modeling shows that DRAGON achieves up to 1.9× greater performance gains over the standalone SLM than the centralized method. Moreover, DRAGON achieves significant reduction in per-token latency compared to synchronized methods, showing strong robustness under various network conditions. Extensive simulations further verify that the proposed scheduling algorithm achieves increasing delay reduction as network latency grows. We summarize the key contributions of this work as follows:

- We propose DRAGON, the first distributed RAG framework that supports distributed documents retrieval and collaborative output generation between cloud and device. It significantly enhances on-device model performance with the integration of both personal and general knowledge.
- We introduce *Speculative Aggregation*, a dual-side speculative algorithm that decouples synchronized aggregation from sequential decoding by asynchronously verifying the output alignment between cloud and device, greatly reducing end-to-end latency.
- We further design an adaptive scheduling algorithm to dynamically identify the optimal aggregation side under varying network conditions, effectively improving decoding efficiency.
- We implement DRAGON in a real-world hardware testbed and perform comprehensive evaluations using representative SLMs and large-scale retrieval corpora, demonstrating significant performance improvements of on-device SLMs with negligible overhead even under high-latency network conditions.

2 Preliminaries

2.1 Retrieval-Augmented Generation

Retrieval-augmented generation [21] integrates off-the-shelf language models with documents retrieved from an external database to capture long-tail knowledge and keep up-to-date with new information. In traditional LM inference, given an input token sequence $x_{<M} = \{x_0, \ldots, x_{M-1}\}$ (indices of tokens in vocabulary V) and the maximum context length N, the output generation process aims to maximize the probability $\prod_{t=M}^{N-1} p(x_t|x_{<t})$. In order to incorporate external documents, we process each document concatenated with the query separately, and then interpolate the output distributions (termed as *output aggregation* [21, 31])[1]. Following the Law of Total Probability, we can derive the interpolation as

$$\boldsymbol{p}(x_t|x_{<t}) = \sum\nolimits_d p(d|x_{<t}) \cdot \boldsymbol{p}(x_t|d, x_{<t}), \tag{1}$$

where $p(d|x_{<t})$ denotes the weight of the document d on the output distribution $\boldsymbol{p}(x_t|d, x_{<t})$. Since $p(d|x_{<t})$ cannot be directly obtained in practice, we retrieve d from a sufficiently large corpus $\mathcal{D}$ and only consider top-k documents with the highest relevance score $\mathcal{R}_{\mathcal{D}}(d, x_{<t})$. Equation (1) offers the opportunity to decompose the multi-document RAG workflow into parallel generation processes, enabling device-cloud distributed RAG. This decomposition also significantly alleviates the limitation of maximum context length on resource-constraint devices.

[1]The output aggregation is different from *context aggregation* [29]), where external documents are concatenated and prepended to the input query $x_{<t}$ all at once.

2.2 Device-Cloud Distributed RAG

To enhance the performance of on-device language model inference, we propose a device-cloud distributed RAG framework based on the above discussed output aggregation paradigm. Given an input $x_{<t}$, we retrieve personalized documents D^{device} from a device-side private database and then compute the next-token distributions $\boldsymbol{P}_t^{\text{device}} = \left[\boldsymbol{p}(x_t|d, x_{<t})\right]^\top_{d\in D^{\text{device}}}$ using an on-device language model $\mathcal{M}^{\text{device}}$. In parallel, we employ a similar process in the cloud and obtain the cloud-side next-token distributions $\boldsymbol{P}_t^{\text{cloud}}$. After gathering all documents $D = D^{\text{device}} \cup D^{\text{cloud}}$ and their corresponding output distributions $\boldsymbol{P}_t = \left[\boldsymbol{P}_t^{\text{device}}, \boldsymbol{P}_t^{\text{cloud}}\right]^\top$, we sample the next token according to

$$x_t \sim \boldsymbol{p}_t = \boldsymbol{\omega}_t^\top \boldsymbol{P}_t = \sum\nolimits_{d\in D} \omega_t(d) \cdot \boldsymbol{p}(x_t|d, x_{<t}), \tag{2}$$

where $\boldsymbol{\omega}_t = \left[\omega_t(d)\right]^\top_{d\in D}$ denotes the interpolation weights, which are computed based on relevance scores $\mathcal{R}$ as

$$\omega_t(d) = \exp \mathcal{R}(d, x_{<t}) / \sum\nolimits_{d'\in D} \exp \mathcal{R}(d', x_{<t}).$$

We refer to this workflow as the vanilla distributed RAG (VDRAG).

Despite its effectiveness, frequent synchronization over network between the device and cloud can introduce a substantial latency. On one hand, the tight data coupling in distributed RAG leads to idle waiting, especially when decoding latencies significantly differ due to hardware heterogeneity. During the auto-regressive language model inference, the output x_{t-1} is expected on both sides as the input for generating $\boldsymbol{P}_t$. At each token generation step t, computing Equation (2) requires waiting for output distributions on both sides ($\boldsymbol{P}_t^{\text{device}}$ and $\boldsymbol{P}_t^{\text{cloud}}$). On the other hand, frequent data transmission makes VDRAG highly sensitive to network latencies. Transmitted data packets at each step includes a 2-byte integer representing the token x_t and a float matrix $\boldsymbol{P}_t$ encoding the output distributions[2]. Due to small data packet size, transmission time is often dominated by data-independent factors [6, 12], like the connection round-trip time (RTT). Finally, idle waiting and transmission latency at each generation step accumulate over a long output sequence, significantly amplifying the overall overhead.

2.3 Problem Formulation

We define the language model inference as a distributed process where the device-side and cloud-side token generation processes, $\mathcal{F}^{\text{device}}$ and $\mathcal{F}^{\text{cloud}}$, executes alternatively. Without loss of generality, we assume the final output token sequence is generated on-device by sampling x from the next-token distribution $\boldsymbol{p}_t$. Let A_t be an auxiliary set for transferring information between the device and the cloud at iteration t, which is initially empty. The workflow can be expressed as $A_t^{\text{device}}, \boldsymbol{p}_t \leftarrow \mathcal{F}^{\text{device}}(A_{t-1}^{\text{cloud}}, \mathcal{M}^{\text{device}}, D^{\text{device}}, x_{<t})$ on the device, and then $A_t^{\text{cloud}} \leftarrow \mathcal{F}^{\text{cloud}}(A_t^{\text{device}}, \mathcal{M}^{\text{cloud}}, D^{\text{cloud}}, x_{<t})$ on the cloud, respectively. Finally, the optimization objective is

$$\min_{\mathcal{F}} \frac{1}{N} \sum\nolimits_{t=1}^{N} \left(-p(x_t^*|x_{<t}) \log \boldsymbol{p}_t(x_t^*|x_{<t}) + \lambda C(A_t, \mathcal{F})\right), \tag{3}$$

where x_t^* represents the optimal token at step t and C denotes the end-to-end latency per token resulted from the transmission of A_t between the device and cloud and the execution of $\mathcal{F}$. The coefficient λ controls the trade-off between performance and efficiency.

[2]The float matrix $\boldsymbol{P}_t$ has a size of $|V| \max(|D^{\text{device}}|, |D^{\text{cloud}}|)$, where the vocabulary size $|V|$ is typically less than 50,000.

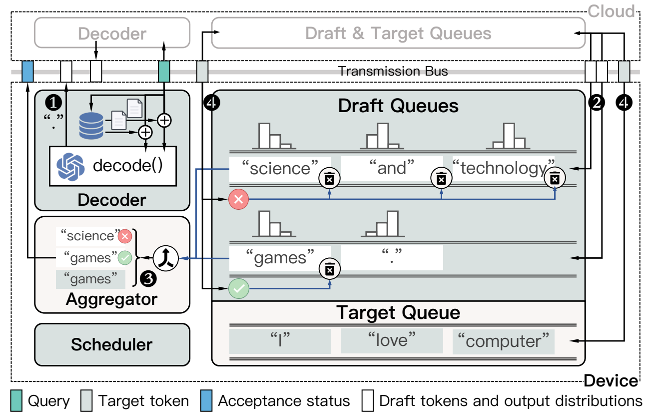

Figure 2: Overview of the DRAGON framework.

3 Overview of DRAGON

To enhance on-device language model inference performance while minimizing the latency overhead, we propose DRAGON, a device-cloud distributed RAG framework. In this framework, we sample tokens from distributions aggregated from the device-side and cloud-side RAG outputs, enabling an integration of personalized information and generic knowledge. To mitigate the inherent latency caused by frequent device-cloud synchronizations in VRAG, we perform distribution aggregation and next-token sampling in a speculative manner, where draft tokens are generated on both sides and then verified on either side. Accordingly, as shown in Figure 2, DRAGON consists of three modules deployed on both sides, including Decoders, Queues, and Schedulers, and an Aggregator module on either side.

We organize Decoders, Queues and Aggregator by a producer-consumer paradigm, enabling asynchronous decoding of draft tokens. The Decoder serves as a token producer, and on each side $s \in \{\text{device}, \text{cloud}\}$ it decodes draft tokens x_t^s independently based on locally-aggregated output distributions $\boldsymbol{p}_t^s = (\tilde{\boldsymbol{\omega}}_t^s)^\top \boldsymbol{P}_t^s$ where $\tilde{\boldsymbol{\omega}}_t = \left[\omega_t(d)\right]^\top_{d\in D^s}$, similar to Equation (2) but using the retrieved local documents D^s only (❶). The draft tokens x_t^s and their corresponding distribution vectors $\boldsymbol{p}_t^s$ are broadcast to the other side. On each side, we enqueue x_t^s into Draft Queues (❷). The Aggregator, as a consumer, continuously consumes draft tokens from the front of local queues and performs aggregation process (❸). Subsequently, the aggregation results of the draft token are broadcast to Draft Queues on both sides. For each queue, the first token is dequeued if accepted, or the entire queue is cleared if rejected. The final target token output by Aggregator is enqueued into Target Queue on both sides (❹). Although the dependencies between the aggregator and decoder cannot be eliminated, the data transmission latency can be overlapped with the decoding time, mitigating the idle waiting. To accommodate dynamic computing resources on both sides and network bandwidth between them, we further design Profilers[3] and Schedulers to identify the optimal aggregation side.

[3]Please refer to our technical report [22] for detailed design of the Profiler.

4 Speculative Aggregation

Inspired by *Speculative Decoding* [20], we propose Speculative Aggregation to reduce the device-cloud communication latency. Speculative Decoding adopts a draft-then-verify decoding paradigm to reduce the number of calls to the resource-intensive LLM. Similarly, Speculative Aggregation utilizes two independent decoding processes, the device-side and cloud-side Decoders, to draft multiple candidate future tokens, which are then verified through an Aggregator. This is equivalent to directly sampling from the distributions aggregated from the device-side and cloud-side outputs. As the aggregation involves collecting output distributions over the network, we expect the speculative algorithm to reduce its frequency and mitigate data transmission costs. More specifically, the Aggregator stays in a blocked wait state until both local Draft Queues are non-empty. Once this condition is met, it retrieves one token $x_t^{\text{device}}/x_t^{\text{cloud}}$ from the front of each queue and fetches corresponding locally-aggregated output distributions $\boldsymbol{p}_t^{\text{device}}/\boldsymbol{p}_t^{\text{cloud}}$ from the cache. The tokens and the distributions are then provided as inputs to the aggregation.

4.1 Design of Aggregation Strategy

Since the workflows of the device and cloud sides are designed to be symmetric, we define $\{l, r\} = \{\text{device}, \text{cloud}\}$ to maintain generality and avoid repetition. From the perspective of the Aggregator, l refers to the local side that performs aggregation, while r denotes the remote side, which only generates draft tokens.

Target distribution. The objective of speculative aggregation is to generate tokens that are equivalent to those sampled from the target distribution $\boldsymbol{p}_t = \boldsymbol{\omega}_t^\top \boldsymbol{P}_t$ as defined in Equation (2). We partition $\boldsymbol{P}_t$ block-wise, grouping its distribution vectors by generation side, and have $\boldsymbol{p}_t = (\boldsymbol{\omega}_t^l)^\top \boldsymbol{P}_t^l + (\boldsymbol{\omega}_t^r)^\top \boldsymbol{P}_t^r$. For each $s \in \{l, r\}$, we have $\boldsymbol{\omega}_t^l = \eta_t^s \tilde{\boldsymbol{\omega}}_t^l$ where $\eta_t^s = h_t^s/(h_t^l + h_t^r)$ and $h_t^s = \sum_{d \in D^s} \exp \mathcal{R}(d, x_{<t})$. As a result, given the locally-aggregated output distributions $\boldsymbol{p}_t^l$ and $\boldsymbol{p}_t^r$, the target distribution $\boldsymbol{p}_t$ can be obtained by an interpolation:

$$\boldsymbol{p}_t = \eta_t^l \boldsymbol{p}_t^l + \eta_t^r \boldsymbol{p}_t^r. \tag{4}$$

To align with this computation process, on each side $s \in \{l, r\}$, a corrected value[4] of h_t^s is computed and retained during decoding x_t^s, and then broadcast and stored along with draft tokens and the locally-aggregated distributions.

Aggregation strategy. To sample $x_t \sim \boldsymbol{p}_t$, we instead perform two independent speculative sampling processes as follows:

- Keep the draft token x_t^l as $\tilde{x}_t^l$ if $\boldsymbol{p}_t^l(x_t^l) \leq \boldsymbol{p}_t^r(x_t^l)$, and in case $\boldsymbol{p}_t^l(x_t^l) > \boldsymbol{p}_t^r(x_t^l)$ we reject the sample with probability $\eta_t^r(1 - \boldsymbol{p}_t^r(x_t^l) \,/\, \boldsymbol{p}_t^l(x_t^l))$ and re-sample $\tilde{x}_t^l$ from an adjusted distribution $\tilde{\boldsymbol{p}}_t^l = \text{norm}(\max(0, \boldsymbol{p}_t^r - \boldsymbol{p}_t^l))$.
- Keep the draft token x_t^r as $\tilde{x}_t^r$ if $\boldsymbol{p}_t^r(x_t^r) \leq \boldsymbol{p}_t^l(x_t^r)$, and in case $\boldsymbol{p}_t^r(x_t^r) > \boldsymbol{p}_t^l(x_t^r)$ we reject the sample with probability $\eta_t^l(1 - \boldsymbol{p}_t^l(x_t^r) \,/\, \boldsymbol{p}_t^r(x_t^r))$ and re-sample $\tilde{x}_t^r$ from an adjusted distribution $\tilde{\boldsymbol{p}}_t^r = \text{norm}(\max(0, \boldsymbol{p}_t^l - \boldsymbol{p}_t^r))$.

Next, we select either $\tilde{x}_t^l$ or $\tilde{x}_t^r$ as x_t with uniform probability. Finally, each draft token x_t^l and x_t^r is accepted if it matches the target token x_t; otherwise, it is rejected. The aggregation strategy at each step t is summarized in Algorithm 1.

Algorithm 1: SpeculativeAggregation

Input: Draft tokens x_t^s, locally-aggregated distributions $\boldsymbol{p}_t^s$, and aggregation weights h_t^s, for $s \in \{l, r\}$
Output: Target token x_t, acceptance status $\mathcal{S}^l$ and $\mathcal{S}^r$

Function `Sample(`x, $\boldsymbol{p}^a$, $\boldsymbol{p}^b$, η`)`**:**
  $\tilde{x} \leftarrow x$, $\sigma^a \sim U(0,1)$;
  if $\boldsymbol{p}^a(x) > \boldsymbol{p}^b(x)$, $\sigma^a < \eta(1 - \boldsymbol{p}^b(x) \,/\, \boldsymbol{p}^a(x))$ **then**
    $\tilde{x} \sim \text{norm}(\max(0, \boldsymbol{p}^b - \boldsymbol{p}^a))$;
  return $\tilde{x}$;
$\eta_t^l \leftarrow h_t^l/(h_t^l + h_t^r)$, $\eta_t^r \leftarrow 1 - \eta_t^l$;
$\tilde{x}_t^l \leftarrow \text{Sample}(x_t^l, \boldsymbol{p}_t^l, \boldsymbol{p}_t^r, \eta_t^r)$, $\tilde{x}_t^r \leftarrow \text{Sample}(x_t^r, \boldsymbol{p}_t^r, \boldsymbol{p}_t^l, \eta_t^l)$;
$\sigma \sim U(0,1)$, $x_t \leftarrow \tilde{x}_t^l \cdot \mathbf{1}_{\sigma \leq 0.5} + \tilde{x}_t^r \cdot \mathbf{1}_{\sigma > 0.5}$;
$\mathcal{S}^l \leftarrow x_t^l = x_t$, $\mathcal{S}^r \leftarrow x_t^r = x_t$;
return $x_t, \mathcal{S}^l, \mathcal{S}^r$;

Theorem 1. *During each generation step t, the target token x_t produced by the speculative aggregation strategy follows a distribution identical to that output by VDRAG.*

Proof. Since the output distribution $\boldsymbol{p}_t$ in Equation (4) is mathematically equivalent to that of VDRAG in Equation (2) through proper matrix partitioning, the theorem can be reformulated as follows: For any pair of locally-aggregated distributions $\boldsymbol{p}_t^l$ and $\boldsymbol{p}_t^r$, the target token x_t is sampled from the convex combination $\boldsymbol{p}_t = \eta_t^l \boldsymbol{p}_t^l + \eta_t^r \boldsymbol{p}_t^r$. Notice that for $s \in \{l, r\}$, the mixture coefficients η_t^s are computed as $\eta_t^s = h_t^s/(h_t^l + h_t^r)$ (see § 4.1 Target distribution), which naturally satisfies the condition $\eta_t^l + \eta_t^r = 1$.

First, we show that the intermediate outputs $\tilde{x}_t^l$ and $\tilde{x}_t^r$ from the two independent speculative sampling processes are indeed drawn from $\boldsymbol{p}_t$. For side l, the probability to reject a draft token is

$$\begin{aligned} P(rejected) &= E_{x \sim \boldsymbol{p}_t^l(x)}(1 - \min(1, \eta_t^l + \eta_t^r \boldsymbol{p}_t^r(x)/\boldsymbol{p}_t^l(x))) \\ &= \eta_t^r \sum (\boldsymbol{p}_t^l(x) - \min(\boldsymbol{p}_t^l(x), \boldsymbol{p}_t^r(x))). \end{aligned}$$

The adjusted distribution, from which we sample after the draft token is rejected, can be expressed as

$$\tilde{\boldsymbol{p}}_t^l(x) = \frac{\boldsymbol{p}_t^r(x) - \min(\boldsymbol{p}_t^l(x), \boldsymbol{p}_t^r(x))}{\sum_{x'} (\boldsymbol{p}_t^r(x') - \min(\boldsymbol{p}_t^l(x'), \boldsymbol{p}_t^r(x')))}.$$

$P(rejected, x = \tilde{x}_t^l)$, the probability that $\tilde{x}_t^l$ is re-sampled after rejecting x_t^l, is

$$P(rejected)\tilde{\boldsymbol{p}}_t^l(\tilde{x}_t^l) = \eta_t^r(\boldsymbol{p}_t^r(\tilde{x}_t^l) - \min(\boldsymbol{p}_t^l(\tilde{x}_t^l), \boldsymbol{p}_t^r(\tilde{x}_t^l))).$$

Consequently, the sampled token $\tilde{x}_t^l$ is drawn from the distribution

$$\begin{aligned} &P(x = \tilde{x}_t^l) = P(accepted, x = \tilde{x}_t^l) + P(rejected, x = \tilde{x}_t^l) \\ &= \boldsymbol{p}_t^l(\tilde{x}_t^l) \min(1, \eta_t^l + \eta_t^r \boldsymbol{p}_t^r(\tilde{x}_t^l) \,/\, \boldsymbol{p}_t^l(\tilde{x}_t^l)) + \eta_t^r(\boldsymbol{p}_t^r(\tilde{x}_t^l) \\ &- \min(\boldsymbol{p}_t^l(\tilde{x}_t^l), \boldsymbol{p}_t^r(\tilde{x}_t^l))) = \eta_t^l \boldsymbol{p}_t^l(\tilde{x}_t^l) + \eta_t^r \boldsymbol{p}_t^r(\tilde{x}_t^l) = \boldsymbol{p}_t(\tilde{x}_t^l). \end{aligned}$$

As a result, $\tilde{x}_t^l$ is distributed identically to tokens sampled from $\boldsymbol{p}_t$. Since the correctness proof for the other side r is symmetric, we can conclude straightforwardly that $\tilde{x}_t^r \sim \boldsymbol{p}_t$. Finally, the aggregation strategy randomly select either $\tilde{x}_t^l$ or $\tilde{x}_t^r$ as the target token x_t, with a uniform probability. Obviously, $x_t \sim 0.5\boldsymbol{p}_t + 0.5\boldsymbol{p}_t = \boldsymbol{p}_t$. □

[4] We adopt the log-sum-exp trick to maintain numerical stability. Details are included in our technical report [22].

To conclude, Speculative Aggregation fundamentally reorders the processing pipeline of VDRAG from aggregate-then-sample to sample-then-aggregate. It first samples from local distributions $\boldsymbol{p}_t^l$ and $\boldsymbol{p}_t^r$ and then aggregates the outputs via a conditional sampling from adjusted distributions followed by the final resampling. This sampling-based aggregation is theoretically necessary to ensure the generated token x_t properly follows the target distribution $\boldsymbol{p}_t$. In contrast, naive binary selection between x_t^l and x_t^r fails to preserve this property. A canonical counterexample occurs in greedy sampling when $\arg\max \boldsymbol{p}_t \notin \{\arg\max \boldsymbol{p}_t^l, \arg\max \boldsymbol{p}_t^r\}$.

Multi-step aggregation. We now present a general procedure for sampling multiple consecutive tokens. At each step t, the following workflow is executed:

1) The Aggregator waits until both Draft Queues are non-empty, then dequeues x_t^s from the local ones and retrieves auxiliary variables $\boldsymbol{p}_t^s$ and h_t^s from the local cache, for each $s \in \{l, r\}$.
2) The Aggregator performs aggregation as defined in Algorithm 1. The outputs, including the target token x_t and the acceptance status of each draft token, are broadcast to notify both sides.
3) Upon receiving the message, each side checks the acceptance status of both x_t^l and x_t^r. If a token is accepted, it is dequeued from the corresponding Draft Queue and step 5) is executed; otherwise, step 4) is executed.
4) If x_t^s is rejected, its corresponding Draft Queues on both sides are cleared and the side s rolls back its KV cache and re-computes the next draft token x_{t+1}^s using the target token x_t as input.
5) Update step $t \leftarrow t + 1$, and go back to step 1).

4.2 Analysis of Acceptance Rate

We now analyze the factors that influence the acceptance rate of draft tokens on both the device and the cloud sides.

Definition 1. *For $s \in \{l, r\}$, the acceptance rate β_t^s, is the probability of accepting $x_t^s \sim \boldsymbol{p}_t^s = \sum_{d \in D^s} \omega_t(d)\boldsymbol{p}(x_t|d, x_{<t})$ by the aggregation strategy, given a prefix $x_{<t}$.*

First, we consider l-side as an example. The acceptance of the draft token x_t^l, sampled from $\boldsymbol{p}_t^l$ by the Decoder, can be classified into two cases: 1) it is accepted during the speculative sampling of $\tilde{x}_t^l$ and 2) the draft token $x_t^r = x_t^l$ is accepted or $\tilde{x}_t^r = x_t^l$ is sampled from $\tilde{\boldsymbol{p}}_t^r$ during the speculative sampling of $\tilde{x}_t^r$. Let γ^l and $\gamma^r = 1 - \gamma^l$ denote weights assigned to $\tilde{x}_t^l$ and $\tilde{x}_t^r$ in the random selection following these sampling processes. We adopt the definition of divergence from [20], given by $\delta = D_{LK}(\boldsymbol{p}_t^l, \boldsymbol{p}_t^r) = 1 - \sum_x \min(\boldsymbol{p}_t^l(x), \boldsymbol{p}_t^r(x))$. The expected acceptance rate $\alpha_t^l = \mathbb{E}_{x \sim \boldsymbol{p}_t^l(x)}(\beta_t^l)$ is computed as

$$\alpha_t^l = \gamma^l(1 - \eta_t^r \delta) + \gamma^r \sum_x \boldsymbol{p}_t^l(x)\boldsymbol{p}_t(x), \tag{5}$$

where the two terms represent the acceptance probability of the two cases above, respectively. These terms are mutually exclusive and their contributions are weighted by the mixture weights γ^l and γ^r (both empirically set to 0.5 in our implementation for simplicity[5]).

Theorem 2. *The expected acceptance rate is influenced by the degree of overlap between the draft distributions on the two sides.*[6]

[5]Please refer to our technical report [22] for design details on random selection weight.
[6]For a detailed analysis of how draft distribution overlap affects acceptance rates, please refer to our technical report [22].

x_{t-1}^l	x_{t-1}^r	**Waiting Time for x_t^l and x_t^r**
rejected	accepted	$\max(c_{\text{dec}}^l, \varphi(c_{\text{dec}}^r + c_{\text{trans}}^r))$
accepted	rejected	$\max(\varphi(c_{\text{dec}}^l), c_{\text{trans}}^l + c_{\text{dec}}^r + c_{\text{trans}}^r)$
accepted	accepted	$\max(\varphi(c_{\text{dec}}^l), \varphi(c_{\text{dec}}^r + c_{\text{trans}}^r))$
rejected	rejected	$\max(c_{\text{dec}}^l, c_{\text{trans}}^l + c_{\text{trans}}^r + c_{\text{dec}}^r)$

Table 1: Waiting time for the next pair of draft tokens x_t^l and x_t^r under different acceptance scenarios of the previous draft tokens x_{t-1}^l and x_{t-1}^r.

This characteristic provides insight into the principle behind *Speculative Aggregation*: we assume that the device-side and cloud-side RAG workflows generate similar results by default, allowing them to asynchronously decode the next tokens without aggregation. Only when they disagree with each other, the acceptance is adjusted by their aggregation weights η_t^l and η_t^r.

5 Greedy Scheduling

To further minimize the latency $C(A_t, \mathcal{F})$ in Equation (3), We adaptively schedule which side performs the next aggregation after the current one is completed. The principle behind this is to maximize the overlap between the device-side and cloud-side decoding and transmission processes, jointly considering dynamic computing resources, network bandwidth, and acceptance of draft tokens. Since predicting future acceptance is challenging due to dynamic document relevance and model outputs, we employ a greedy strategy, where at each step, we minimize the expected latency per token based on current observations.

The latency per token, denoted as Z_t, is computed as the average duration between two consecutive aggregations. It can be viewed as the waiting time for the next pair of draft tokens, x_t^{device} and x_t^{cloud}, including both decoding and transmission delays, as the aggregation duration is negligible. For each side $s \in \{\text{device}, \text{cloud}\}$, let c_{dec}^s denote the decoding delay of a draft token x_t^s, and c_{trans}^s denote the transmission delay of this token and its auxiliary variables from s to the other side. Since the decoding and transmission processes are asynchronous, they may still be ongoing when the scheduling algorithm is executed. Therefore, we define $\varphi(T_{\text{total}}(u)) = \max(0, T_{\text{total}}(u) + T_{\text{begin}}(u) - T_{\text{now}})$ as a function that estimates the remaining time of the total duration T_{total} to complete the process u, where T_{begin} and T_{now} are the beginning and current timestamps, respectively. Let l be the side that currently performs aggregation and r be the other one. The best side is then selected as

$$s^* = \arg\min_{s \in \{l, r\}} Z_t^s(\varphi, c_{dec}^l, c_{trans}^l, c_{dec}^r, c_{trans}^r), \tag{6}$$

where Z_t^s denotes the latency per token when s continuously performs the aggregations in the future.

Next, we present the calculation of Z_t^s. Table 1 illustrates the waiting time for the next pair of draft tokens after a previous aggregation. To estimate an averaged Z_t^s over multiple future steps, rather than enumerating all possible combinations of acceptance scenarios, we assume each acceptance scenario repeats continuously[7] and occurs with an expected probability given by the acceptance rate. Therefore, the waiting time in Table 1 can be simplified to eliminate the function φ. First, assuming that draft tokens from r are always accepted, the decoding process for consecutive draft tokens will be

[7]Please refer to our technical report [22] for pipeline illustrations of different cases.

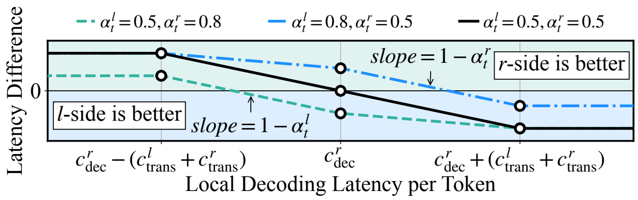

Figure 3: Difference in per-token latencies when side l and r performs aggregation, versus varying l-side decoding latency.

continuous on r. In other words, the decoding of x_t^r begins exactly when x_{t-1}^r is decoded and ready for transmission. Therefore, we have $\varphi(c_{\text{dec}}^r + c_{\text{trans}}^r) = (T_{\text{begin}} + c_{\text{trans}}^r - T_{\text{now}}) + c_{\text{dec}}^r = c_{\text{dec}}^r$. Moreover, since the aggregation process can exhaustively consume the token pairs in the Draft Queues, $\varphi(c_{\text{dec}}^l) < c_{\text{dec}}^l$ holds only when the waiting time for x_t^r dominates. Hence, $\max(\varphi(c_{\text{dec}}^l), \cdot) = \max(c_{\text{dec}}^l, \cdot)$. Finally, Z_t^l is calculated as

$$\alpha_t^r \max(c_{\text{dec}}^l, c_{\text{dec}}^r) + (1-\alpha_t^r)\max(c_{\text{dec}}^l, c_{\text{dec}}^r + c_{\text{trans}}^l + c_{\text{trans}}^l). \quad (7)$$

Symmetrically, Z_t^r is computed by exchanging l and r in Equation (7). Based on this, we can conclude that when the local decoding latency c_{dec}^l cannot cover the waiting time for draft tokens from the other side, i.e., $c_{\text{dec}}^l < c_{\text{dec}}^r + c_{\text{trans}}^l + c_{\text{trans}}^l$, minimizing the overall latency Z_t^l requires maximizing the acceptance rate α_t^r.

To decide the optimal side in Equation (6), we calculate the difference in latencies per token when side l and r performs aggregation. The result is presented as a piecewise function,

$$\Delta Z_t = \begin{cases} (1-\alpha_t^r)\text{rtt}, & c_{\text{dec}}^l \le c_{\text{dec}}^r - \text{rtt} \\ (1-\alpha_t^l)j + (\alpha_t^l - \alpha_t^r)\text{rtt}, & c_{\text{dec}}^r - \text{rtt} < c_{\text{dec}}^l \le c_{\text{dec}}^r \\ (1-\alpha_t^r)j + (\alpha_t^l - \alpha_t^r)\text{rtt}, & c_{\text{dec}}^r < c_{\text{dec}}^l \le c_{\text{dec}}^r + \text{rtt} \\ (a_t^l - 1)\text{rtt}, & c_{\text{dec}}^r + \text{rtt} < c_{\text{dec}}^l \end{cases}, \quad (8)$$

where $\text{rtt} = c_{\text{trans}}^l + c_{\text{trans}}^r$, and j is the difference in decoding latencies, $c_{\text{dec}}^r - c_{\text{dec}}^l$. Accordingly, we select side r for aggregation when $\Delta Z_t > 0$, and side l otherwise. Figure 3 shows the influence of varying acceptance rates on ΔZ_t. As the acceptance rate of draft tokens from one side increases, the Scheduler tends to favor the opposite side. Moreover, the relationship between c_{dec}^l and c_{dec}^r also influences the strategy. For instance, when the decoding process on one side becomes the latency bottleneck, aggregation is always performed on that side, which is demonstrated by $(1-\alpha_t^r)\text{rtt} \ge 0$ and $(\alpha_t^l - 1)\text{rtt} \le 0$. Clearly, our strategy minimizes the likelihood of repeated bottleneck decoding due to rejection, while maximizing the overlap between the decoding and transmission processes.

6 Theoretical Analysis

In this section, we present a theoretical analysis to demonstrate the improvement in wall-time efficiency achieved by DRAGON over VDRAG described in § 2.2. To facilitate analysis, we assume the aggregation is always performed on the device in following discussions and l = device and r = cloud.

First, we illustrate two boundary conditions of DRAGON using pipeline graphs: 1) the optimal case where all draft tokens from both device and cloud sides are accepted (Figure 4a), and 2) the worst case where all draft tokens are rejected (Figure 4b). For our case study, device and cloud decoding latencies are 2 s and 1 s,

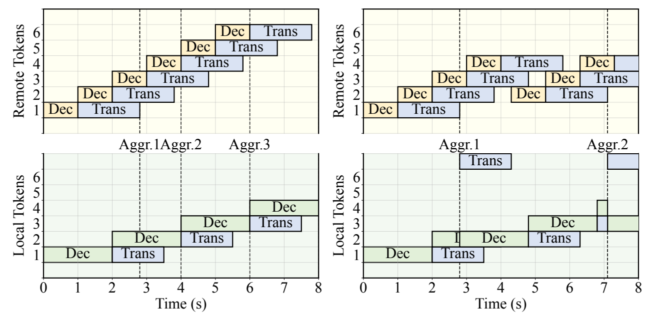

(a) Accept **(b) Reject**

Figure 4: Decoding pipelines when the Aggregator continuously accepts/rejects both x^l and x^r.

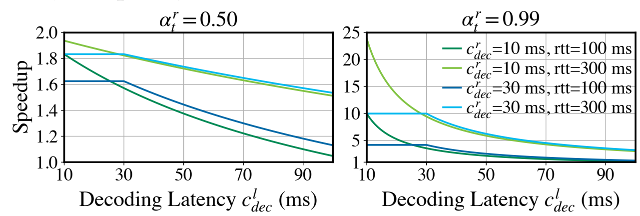

Figure 5: Theoretical speedup of DRAGON compared to the vanilla distributed RAG vs. varying c_{dec}^l, c_{dec}^r, rtt and α_t^r.

respectively, with asymmetric network delays of 1.5 s (device-to-cloud) and 1.8 s (cloud-to-device). We assume the two sides start decoding at the same time. In the optimal case, when the device and cloud exchange their initial draft tokens at 2.8 s and 3.5 s, respectively, mutual acceptance occurs. This successful speculation enables uninterrupted continuous decoding of subsequent tokens, ultimately achieving a stable end-to-end per-token decoding latency of 2 s after two synchronization rounds. In the worst case, the device receives the cloud's first draft token at 2.8 s, triggering immediate aggregation with its local draft token followed by target token sampling. Since both draft tokens are rejected, the system must abort the ongoing second-token decoding and roll back to recompute the second token using the initial target token. The cloud subsequently encounters an identical failure mode at 4.3 s. These cascading speculation failures ultimately produce a substantially degraded per-token latency of 4.3 s.

As established in § 4.1, VDRAG yields identical output distributions to DRAGON. It decodes the next token only when the device-side and cloud-side draft token pair becomes available, inherently matching the latency profile of DRAGON's worst-case scenario[8], where continuous decoding with full rollback occurs. The pipeline diagrams demonstrate that in the optimal case, continuous daft decoding effectively hides transmission latency through perfect speculation and enables significantly lower end-to-end per-token latency. This reveals DRAGON's fundamental advantages over VDRAG in terms of potential latency reduction.

Building upon these observations, we now present a formal theoretical analysis to quantify this performance improvement.

Definition 2. *Let Z_t and $\tilde{Z}_t$ be the expected per-token latencies at step t when using DRAGON and the vanilla distributed RAG, respectively. Define the speedup as $S_t = \tilde{Z}_t / Z_t$.*

[8] DRAGON yields negligible transmission overhead compared to VDRAG. (See § 7.3)

Theorem 3. *Let l = device and r = cloud denote the local and remote computing nodes, respectively. The speedup factor can be formally expressed as a piecewise function of the decoding latencies (c^l_{dec}, c^r_{dec}) and the round-trip communication delay rtt, as follows:*

$$\frac{1}{S_t} = \begin{cases} 1 - \frac{\alpha^r_t}{1+c^r_{dec}/rtt}, & c^l_{dec} \le c^r_{dec}, \\ 1 - (1 - \frac{c^l_{dec}}{c^r_{dec}+rtt})\alpha^r_t, & c^r_{dec} < c^l_{dec} \le c^r_{dec} + rtt, \\ 1, & c^r_{dec} + rtt < c^l_{dec} \end{cases} \tag{9}$$

Proof. Z_t is computed according to Equation (7). By substituting $\alpha^l_t = \alpha^r_t = 0$ and we obtain $\tilde{Z}_t = \max(c^l_{\text{dec}}, c^r_{\text{dec}} + \text{rtt})$. The result then follows from a simple case-by-case analysis. □

Figure 5 illustrates the theoretical speedup characterized in Theorem 3. The speedup achieves its maximum when the device-side decoding latency is minimal and maintains saturated until it surpasses that of the cloud. Thereafter, the speedup decreases inversely with c^l_{dec}, gradually approaching 1 and eventually stabilizing at 1 once c^l_{dec} exceeds c^r_{dec} + rtt. Finally, we have following corollaries:

Corollary 1. *DRAGON is particularly effective when the decoding latency gap between the device and the cloud is small and the transmission cost becomes the primary bottleneck.*

This characteristic extends DRAGON's applicability to distributed computing paradigms with balanced computational capabilities across nodes, while making it particularly suitable when network communication becomes the dominant performance constraint requiring optimization.

Corollary 2. *DRAGON's improvement in wall time can be substantially amplified when the cloud-side acceptance rate is high.*

DRAGON introduces speculative execution by sampling draft tokens directly from locally-aggregated output distributions, rather than waiting for device-cloud aggregated target tokens. This enables uninterrupted auto-regressive decoding by immediately using the sampled draft token as input for subsequent generation. The draft sampling introduces negligible computation and communication overhead, enabling DRAGON to maintain strict latency parity with VDRAG in the worst case. In typical cases where draft tokens are accepted, DRAGON achieves significantly lower end-to-end latency, which has been verified in our experiments in § 7.3. Moreover, prior work [41] shows that most attention focuses on a critical token subset whose modification substantially alters outputs. We observe draft discrepancies mainly arise from this subset, while context-independent tokens (stop words, punctuation, common terms) achieve high acceptance rates due to their shared nature.

7 Experiments

7.1 Implementation

We implemented DRAGON for distributed RAG workflow comprising ~3,000 lines of Python code.[9] The System consists of two symmetric processes, the device-side and cloud-side ones, each utilizing eight threads for core functionalities (e.g., decoding, aggregation and transmission) along with a memory-resident service process for document retrieval. We implemented information synchronization between threads using multi-producer, multi-consumer queues, and between processes using socket-based communication.

7.2 Experiment Setups

Testbed. We evaluated our framework and baseline methods using a high-performance computer as the cloud server and a MacBook Pro as the edge device. The server is equipped with an Intel Xeon Silver 4210R CPU, 64GB of memory, and a GeForce RTX 3090 GPU, while the MacBook Pro features an Intel Core i7 CPU, 16GB of memory, and no dedicated GPU. The cloud and the device are connected via a 2.4 GHz Wi-Fi local-area network, with latency and jitter measured by sockperf as 2ms and 6ms, respectively. To simulate network jitter, we replay a predefined random latency trace by adjusting the network interface controller (NIC) latency using the traffic control tool, *tc*.

Datasets and metrics. We evaluated the long-sequence generation performance of DRAGON on the large-scale language modeling dataset WikiText [25], which comprises over 100 million tokens extracted from verified Good and Featured articles on Wikipedia. We constructed retrieval corpora from the training sets of two different-scale versions, WikiText2 and WikiText103. During evaluation, we applied rolling windows of 1024 and 512 tokens, respectively, over their test sets, using the first 1/8 of each window as the query for retrieval and the remaining tokens for perplexity evaluation. To further assess the efficiency of our method, we measure the time to first token (TTFT) and per-token latency. In this measurement, we used the retrieval corpus and index pre-built by Facebook from a Wikipedia dump dated December 20, 2018, which contains 21 million documents.

Models and baselines. We used OPT-1.3B [40] and Qwen2.5-1.5B [34], with vocabulary sizes of 151,936 and 50,272, respectively. For language modeling and latency measurement, we adopted Contriever [14] and DPR [17] as the retrievers, respectively. Additionally, we employed ms-marco-MiniLM-L6-v2 [30] for document reranking. We compare DRAGON with four baseline methods:

- CRCG, centralized generation augmented with centralized retrieval from local corpus, using the context-aggregation strategy, which represents most existing RAG methods [15, 23, 29].
- DRCG, on-device generation augmented with documents retrieved from a distributed corpus spanning both the device and the cloud, using the context-aggregation strategy.
- DRDG/TW, distributed RAG using the output aggregation strategy and token-wise synchronization, namely VDRAG, as discussed in § 2.2. The target tokens are collected and aggregated on the device side.
- DRDG/SW, distributed RAG using the output aggregation strategy and sequence-wise synchronization, i.e., one-time aggregation of the independently generated output sequences from the device and the cloud. This baseline is implemented by extending the official REPLUG [31] implementation and Facebook's RAG-Sequence model [21] with distributed support.

To simulate insufficient but complementary corpus in the cloud and device sides, we constrain the on-cloud and on-device retrieval by selecting the first and second halves of the top-k documents from the same corpus, respectively. Moreover, to study the overhead of DRCG, we evaluate two variants: DRCG/Text retrieves raw text and

[9] Our code is available at GitHub [22]. Please refer to our technical report for more implementation details.

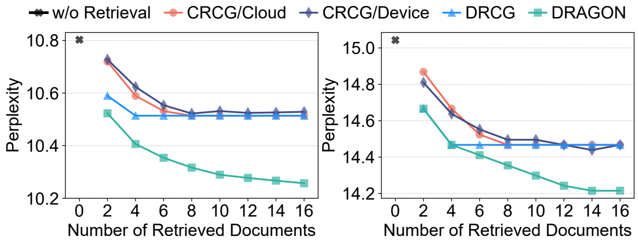

(a) Qwen2.5-1.5B/WikiText2. (b) OPT-1.3B/WikiText103.

Figure 6: Performance on WikiText.

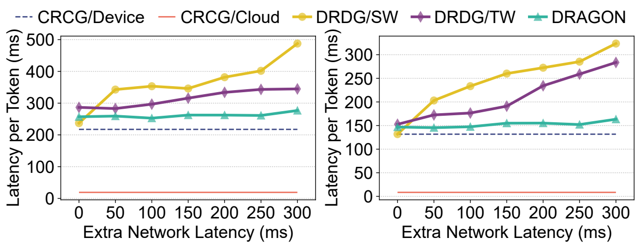

(a) Qwen2.5-1.5B. (b) OPT-1.3B.

Figure 7: Per-token latency in various network conditions.

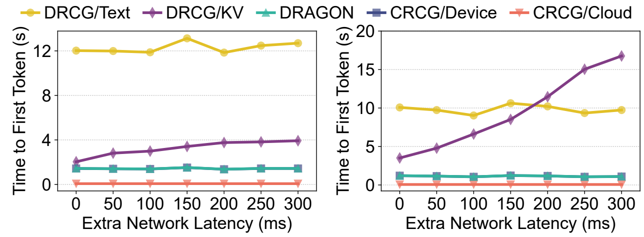

(a) Qwen2.5-1.5B. (b) OPT-1.3B.

Figure 8: Time-to-First-Token in various network conditions.

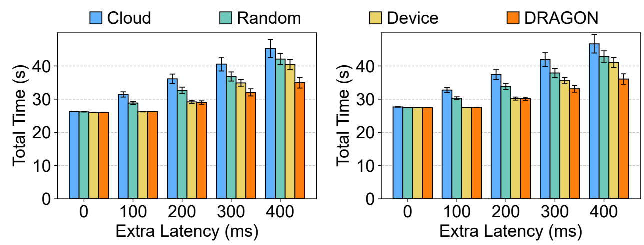

(a) Qwen2.5-1.5B. (b) OPT-1.3B.

Figure 9: Comparison of different scheduling strategies.

prefill KV cache from scratch and DRCG/KV retrieves and reuses the KV cache of documents directly.

7.3 Overall Performance and Efficiency

We first present the overall performance and efficiency of DRAGON in comparison to the baselines. In the following experiments, we set the maximum context length to 256 tokens on both the device and cloud sides, with each retrieved document limited to 64 tokens.

Performance. We linearly increase the number of retrieved documents on both sides from 0 to 16 and report the corresponding language modeling perplexity on WikiText. As shown in Figure 6, DRAGON matches or outperforms all baseline methods across all settings. As more documents are integrated, the performance gap between DRAGON and the baseline methods widens. Finally, DRAGON achieves 1.9× and 1.4× improvements over the non-RAG method, compared to the second-best RAG baselines, for Qwen and OPT, respectively. In contrast, CRCG methods perform poorly due to an insufficient number of retrieved documents, which indicates incomplete knowledge for the given context. Additionally, the performance of DRCG quickly saturates once the amount of retrieved text reaches the context budget limit. However, we observe a gap between DRCG and our method prior to the saturation, suggesting that output aggregation may inherently outperform context aggregation. The results of DRDG methods are omitted, as they produce identical outputs to DRAGON under the language modeling setting.

Efficiency. We inject additional latency to the server's NIC, ranging from 0 to 300 ms, along with a jitter equal to 1/5 of the corresponding latency value. We sample prompts from *10k_prompts_ranked* [13], a collection of synthetic and human-generated prompts with associated ranking, and report the average end-to-end decoding latency over 20 output tokens[10]. Figure 7 presents the per-token latency when incorporating the top-2 relevant documents for the RAG process on each side. As shown in the figure, DRAGON demonstrates strong robustness under different network conditions compared to other distributed baseline methods. Specifically, DRAGON achieves latency reduction of 49.5% and 42.4% when using OPT-1.3B compared to the sequence-wise and token-wise DRDG methods, respectively. In contrast, the per-token latency of DRDG methods fluctuates significantly and tends to increase under higher network latency conditions. Sequence-wise DRDG collects output distributions of all tokens once after generation completes, resulting in a one-time large data transmission and increased sensitivity to network latency. Token-wise DRDG amortizes data transmission over the entire generation process, partially hiding latency within decoding. However, it still under-performs compared to DRAGON due to frequent output synchronizations. Additionally, DRCG methods yields the same per-token latency with corresponding CRCG methods, because they do not involve cooperation between the device and the cloud. Although DRAGON incurs an average latency overhead of 15.6%–20.3% compared to device-only methods, it effectively supports tasks that require both personal and general knowledge, where device-only or cloud-only methods may fail.

We further compare the TTFT of DRAGON with that of the baseline methods under identical network conditions. TTFT typically includes the time for document retrieval and the latency of the prefill stage, during which the key-value (KV) activations for the concatenation of retrieved documents and the input query are either computed from scratch in parallel or loaded from cache. As shown in Figure 8, DRAGON incurs negligible TTFT overhead compared to the device-only CRCG method. In contrast, as KV cache is hosted on the same side with the corpus, DRCG/Text performs prefill from scratch, resulting in high computation latency and 8.6× TTFT on average compared to DRAGON. DRCG/KV directly fetches KV activations from the server, leading to increased transmission time under higher network latency and yielding over 15.3× TTFT compared to DRAGON, rendering it entirely impractical. Notably,

[10]Despite averaging, the results still exhibits fluctuations due to varying CPU load and network jitter, but do not affect the overall conclusion.

DRCG/Text incurs larger prefill latency when using Qwen2.5-1.5B compared to OPT-1.3B, due to its larger number of parameters. In contrast, DRCG/KV exhibits higher TTFT on OPT-1.3B, as Qwen2.5-1.5B employs Grouped-Query Attention [2] to reduce the size of KV activations. The transmission data size in DRCG/KV is 114 MB/16 MB for OPT-1.3B/Qwen2.5-1.5B when retrieving 2 documents of 64 tokens each. Local document retrieval latency is measured at 52.6 ms, while latency for remote raw-text retrieval ranges from 107.2 ms to 745.2 ms as extra network latency increases from 0 to 300 ms.

7.4 Effectiveness of Scheduling

To thoroughly evaluate the effectiveness of scheduling, we implemented a simulator to run DRAGON repeatedly using different scheduling strategies under consistent settings. We compare our scheduling strategy with three baseline methods: (1) *Cloud* and (2) *Device*, where aggregation is statically performed in the cloud and the device, respectively, and (3) *Random*, which randomly selects the side for aggregation. To implement the simulation, we record and replay the acceptance decisions of the Aggregator, and use real-world measurements of decoding latency on each side. We simulate varying network conditions by adding an extra latency and a sinusoidal jitter to the measured base latency. The period of the jitter is set to 20π seconds with its amplitude set to 1/5 of the corresponding latency, consistent with the settings in § 7.3.

Figure 9 presents the total time required to generate 100 tokens under varying network conditions, each averaged over 50 different acceptance decision sequences. The results show that DRAGON's scheduling strategy matches or outperforms all baselines across all settings, with the efficiency gains increasing as the extra latency grows. Due to the substantial gap in decoding latencies between the device and the cloud (as shown in Figure 7), performing aggregation on the device naturally hides cloud-side decoding and transmission within device-side decoding. When network latency is low, *Cloud* and *Random* tend to incur higher latency while DRAGON consistently selects the device side for aggregation. As network latency grows and transmission becomes the bottleneck, DRAGON dynamically selects the side with higher acceptance rate to minimize transmission resulted from draft rejection. Finally, we argue that when device-side and cloud-side decoding latencies become closer in value, the overall generation time will be more sensitive to the network latency. In that case, our scheduling strategy will achieve greater improvement compared to these baseline methods.

Case study. To illustrate DRAGON's detailed scheduling process, we present a 15-token snapshot of a random simulation with the extra latency set to 500 ms. Figure 10 shows, from top to bottom, the cloud-side and device-side generation pipelines, the instantaneous RTT, the estimation score ΔZ as defined in Equation (8), and the accumulated acceptance rates. The pipeline graph comprises vertically arranged bars representing decoding and different transmission tasks (including transmission of draft tokens, target tokens and instruction signals for switching aggregation place).

Initially, the Aggregator resides on the device by default. From the perspective of the device, $c^r_{\text{dec}} < c^l_{\text{dec}} \leq c^r_{\text{dec}} + \text{rtt}$ consistently holds and ΔZ is computed as the sum of two terms, $A = (1 - \alpha^r_t)(c^r_{\text{dec}} - c^l_{\text{dec}})$ and $B = (\alpha^l_t - \alpha^r_t)\text{rtt}$. After the first aggregation at 0.5 s, the acceptance rates are updated to $\alpha^l_0 = 1$ and $\alpha^r_0 = 0$. As a result, the positive term B dominates and $\Delta Z > 0$. The Scheduler decides

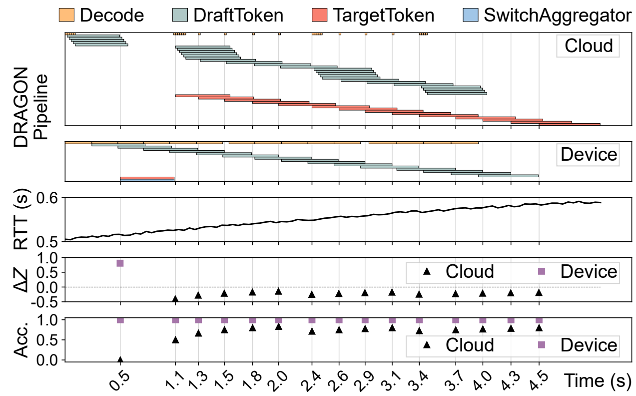

Figure 10: A random snapshot of the generation pipeline and scheduling decisions of DRAGON.

to switch the Aggregator to the cloud, sending the switching signal along with the target token. It then shifts to the cloud's perspective and reverses the sign of ΔZ. Subsequently, since the accumulated cloud-side acceptance rate remains lower, the Scheduler continues to estimating $\Delta Z < 0$, indicating that cloud-side aggregation is more efficient. This case shows that DRAGON's scheduling strategy dynamically minimizes decoding and transmission costs on the side with a lower acceptance rate, which is consistent with our analysis in § 5 and the results shown in Figure 9.

7.5 Overhead Analysis

DRAGON introduces an additional sampling operation at each decoding step. However, as illustrated by the *Sample* function in Algorithm 1, the overhead is minimal, involving only two scalar-level random generations, subtractions, multiplications, and comparisons, along with one vector-level subtraction, comparison, and normalization. Taking Qwen2.5-1.5B (the model used in our evaluation with an output vocabulary size of 151,936) as an example, the extra computational cost of sampling is less than 3×10^5 multiply-accumulate operations (MACs), which takes ~1 us and is negligible compared to the $>10^9$ MACs required for decoding a single token.

Regarding communication overhead, our efficient data compression strategy [22] ensures that transmitting the output distributions incurs less than 0.5 KB of extra data per token. Under a 100 Mbps local-area Wi-Fi network, this translates to <40 us of transmission latency, which is also negligible.

8 Related Works

RAG with Multiple Documents. Existing approaches aggregate retrieved documents via either *output aggregation* (effective for encoder-only and seq2seq models [11, 21] and adapted to decoder-only LLMs [31]) or *context aggregation* (prepend the concatenation of all documents to the input for simplicity [15, 23, 29]). Our framework leverages *output aggregation* to facilitate the decomposition of the multi-document RAG workflow across the device and the cloud, whereas existing works adopt a centralized architecture.

Device-Cloud Collaborative Inference. While prior work [3, 19, 39] established device-cloud collaborative inference for conventional neural networks, recent extensions to LLMs [27, 28] remain limited in privacy-preserving RAG. Hybrid-RACA [36] retrieves and compresses cloud documents for on-device SLMs, while [10] enhances kNN-LMs [18] using cloud interaction history. Both approaches prioritize availability over privacy by processing single-source LLM outputs. In contrast, DRAGON leverages databases on both the device and cloud sides, enabling model collaboration without compromising document privacy.

Speculative Decoding. First proposed in [35], this technique employs a SLM to draft multiple future tokens for parallel verification by the target LLM. Variants include Speculative Sampling [7, 20] for diverse sampling strategies, and approaches like Medusa [5] and Blockwise Decoding [33] that use modified Transformer decoders for parallel drafting. Other work [37, 38] implements drafting via early exiting. In contrast to speculative decoding, where a single drafter fast predicts the output of the target LLM, speculative aggregation in DRAGON verifies the consistency between outputs generated by two distinct LLMs.

9 Conclusion

To address privacy risks of cloud LLMs and limited capabilities of on-device SLMs, we propose DRAGON, a distributed RAG framework that enhances on-device SLMs using both personal and general knowledge without raw document transmission between the device and the cloud. DRAGON partitions the RAG workflow across device and cloud, using *Speculative Aggregation* to minimize output synchronization overhead. Experimental results show that DRAGON notably improves generation quality while maintaining low latency.

References

[1] Abdelrahman Abouelenin, Atabak Ashfaq, Adam Atkinson, Hany Awadalla, Nguyen Bach, Jianmin Bao, Alon Benhaim, Martin Cai, Vishrav Chaudhary, Congcong Chen, et al. 2025. Phi-4-Mini Technical Report: Compact yet Powerful Multimodal Language Models via Mixture-of-LoRAs. arXiv:2503.01743

[2] Joshua Ainslie, James Lee-Thorp, Michiel de Jong, Yury Zemlyanskiy, Federico Lebrón, and Sumit Sanghai. 2023. GQA: Training Generalized Multi-Query Transformer Models from Multi-Head Checkpoints. In *EMNLP*. 4895–4901.

[3] Amin Banitalebi-Dehkordi, Naveen Vedula, Jian Pei, Fei Xia, Lanjun Wang, and Yong Zhang. 2021. Auto-Split: A General Framework of Collaborative Edge-Cloud AI. In *SIGKDD*. 2543–2553.

[4] Sebastian Borgeaud, Arthur Mensch, Jordan Hoffmann, Trevor Cai, Eliza Rutherford, et al. 2022. Improving Language Models by Retrieving from Trillions of Tokens. In *ICML*. 2206–2240.

[5] Tianle Cai, Yuhong Li, Zhengyang Geng, Hongwu Peng, Jason D. Lee, Deming Chen, and Tri Dao. 2024. Medusa: Simple LLM Inference Acceleration Framework with Multiple Decoding Heads. In *ICML*. 5209–5235.

[6] Neal Cardwell, Yuchung Cheng, C Stephen Gunn, Soheil Hassas Yeganeh, and Van Jacobson. 2016. BBR: Congestion-Based Congestion Control: Measuring bottleneck bandwidth and round-trip propagation time. *Queue* 14 (2016), 20–53.

[7] Charlie Chen, Sebastian Borgeaud, Geoffrey Irving, Jean-Baptiste Lespiau, Laurent Sifre, and John Jumper. 2023. Accelerating Large Language Model Decoding with Speculative Sampling. arXiv:2302.01318

[8] Jiawei Chen, Hongyu Lin, Xianpei Han, and Le Sun. 2024. Benchmarking Large Language Models in Retrieval-Augmented Generation. In *AAAI*. 17754–17762.

[9] DeepSeek-AI. 2024. DeepSeek-V3 Technical Report. arXiv:2412.19437

[10] Yucheng Ding, Chaoyue Niu, Fan Wu, Shaojie Tang, Chengfei Lyu, and Guihai Chen. 2024. Enhancing On-Device LLM Inference with Historical Cloud-Based LLM Interactions. In *SIGKDD*. 597–608.

[11] Kelvin Guu, Kenton Lee, Zora Tung, Panupong Pasupat, and Mingwei Chang. 2020. Retrieval Augmented Language Model Pre-Training. In *ICML*. 3929–3938.

[12] Junxian Huang, Feng Qian, Alexandre Gerber, Z Morley Mao, Subhabrata Sen, and Oliver Spatscheck. 2012. A Close Examination of Performance and Power Characteristics of 4G LTE Networks. In *MobiSys*. 225–238.

[13] Data is Better-Together. 2024. 10k_prompts_ranked. https://huggingface.co/datasets/data-is-better-together/10k_prompts_ranked. Accessed: 2025-03-31.

[14] Gautier Izacard, Mathilde Caron, Lucas Hosseini, Sebastian Riedel, Piotr Bojanowski, Armand Joulin, and Edouard Grave. 2021. Unsupervised Dense Information Retrieval with Contrastive Learning. https://arxiv.org/abs/2112.09118

[15] Zhengbao Jiang, Frank Xu, Luyu Gao, Zhiqing Sun, Qian Liu, Jane Dwivedi-Yu, Yiming Yang, Jamie Callan, and Graham Neubig. 2023. Active Retrieval Augmented Generation. In *EMNLP*. 7969–7992.

[16] Peter Kairouz, H Brendan McMahan, Brendan Avent, Aurélien Bellet, Mehdi Bennis, Arjun Nitin Bhagoji, Kallista Bonawitz, Zachary Charles, Graham Cormode, Rachel Cummings, et al. 2021. Advances and Open Problems in Federated Learning. *Foundations and Trends in Machine Learning* 14, 1–2 (2021), 1–210.

[17] Vladimir Karpukhin, Barlas Oğuz, Sewon Min, Patrick Lewis, Ledell Wu, Sergey Edunov, Danqi Chen, and Wen-tau Yih. 2020. Dense Passage Retrieval for Open-Domain Question Answering. In *EMNLP*. 6769–6781.

[18] Urvashi Khandelwal, Omer Levy, Dan Jurafsky, Luke Zettlemoyer, and Mike Lewis. 2020. Generalization through Memorization: Nearest Neighbor Language Models. In *ICLR*.

[19] Stefanos Laskaridis, Stylianos I Venieris, Mario Almeida, Ilias Leontiadis, and Nicholas D Lane. 2020. SPINN: Synergistic Progressive Inference of Neural Networks over Device and Cloud. In *MobiCom*. 1–15.

[20] Yaniv Leviathan, Matan Kalman, and Yossi Matias. 2023. Fast Inference From Transformers via Speculative Decoding. In *ICML*. 19274–19286.

[21] Patrick Lewis, Ethan Perez, Aleksandra Piktus, Fabio Petroni, Vladimir Karpukhin, Naman Goyal, Heinrich Küttler, Mike Lewis, Wen-tau Yih, Tim Rocktäschel, et al. 2020. Retrieval-Augmented Generation for Knowledge-Intensive NLP Tasks. In *NIPS*. 9459–9474.

[22] Shangyu Liu. 2025. *DRAGON: A Device-Cloud Distributed RAG Framework that Enables a Simultaneous Integration of Personalized Information and Generic Knowledge.* https://github.com/ThomasAtlantis/DRAGON

[23] Hongyin Luo, Tianhua Zhang, Yung-Sung Chuang, Yuan Gong, Yoon Kim, Xixin Wu, Helen Meng, and James Glass. 2023. Search Augmented Instruction Learning. In *EMNLP*. 3717–3729.

[24] Yu Ma, Weifa Liang, Jing Li, Xiaohua Jia, and Song Guo. 2020. Mobility-Aware and Delay-Sensitive Service Provisioning in Mobile Edge-Cloud Networks. *TMC* 21, 1 (2020), 196–210.

[25] Stephen Merity, Caiming Xiong, James Bradbury, and Richard Socher. 2017. Pointer Sentinel Mixture Models. In *ICLR*.

[26] OpenAI. 2023. GPT-4 Technical Report. arXiv:2303.08774

[27] Yanghe Pan, Zhou Su, Yuntao Wang, Shaolong Guo, Han Liu, Ruidong Li, and Yuan Wu. 2024. Cloud-Edge Collaborative Large Model Services: Challenges and Solutions. *IEEE Network* 39, 4 (2024), 182–191.

[28] Guanqiao Qu, Qiyuan Chen, Wei Wei, Zheng Lin, Xianhao Chen, and Kaibin Huang. 2024. Mobile Edge Intelligence for Large Language Models: A Contemporary Survey. arXiv:2407.18921

[29] Ori Ram, Yoav Levine, Itay Dalmedigos, Dor Muhlgay, Amnon Shashua, Kevin Leyton-Brown, and Yoav Shoham. 2023. In-Context Retrieval-Augmented Language Models. *TACL* 11 (2023), 1316–1331.

[30] Nils Reimers and Iryna Gurevych. 2019. Sentence-BERT: Sentence Embeddings using Siamese BERT-Networks. In *EMNLP*. 3980–3990.

[31] Weijia Shi, Sewon Min, Michihiro Yasunaga, Minjoon Seo, Rich James, Mike Lewis, Luke Zettlemoyer, and Wen-tau Yih. 2024. REPLUG: Retrieval-Augmented Black-Box Language Models. In *NAACL*. 8371–8384.

[32] Milad Shokouhi, Luo Si, et al. 2011. Federated Search. *Foundations and Trends in Information Retrieval* 1 (2011), 1–102.

[33] Mitchell Stern, Noam Shazeer, and Jakob Uszkoreit. 2018. Blockwise Parallel Decoding for Deep Autoregressive Models. In *NIPS*. 10107–10116.

[34] Qwen Team. 2024. Qwen2.5 Technical Report. arXiv:2412.15115

[35] Heming Xia, Tao Ge, Peiyi Wang, Si-Qing Chen, Furu Wei, and Zhifang Sui. 2023. Speculative Decoding: Exploiting Speculative Execution for Accelerating Seq2seq Generation. In *EMNLP*. 3909–3925.

[36] Menglin Xia, Xuchao Zhang, Camille Couturier, Guoqing Zheng, Saravan Rajmohan, and Victor Rühle. 2024. Hybrid-RACA: Hybrid Retrieval-Augmented Composition Assistance for Real-time Text Prediction. In *EMNLP*. 120–131.

[37] Seongjun Yang, Gibbeum Lee, Jaewoong Cho, Dimitris Papailiopoulos, and Kangwook Lee. 2024. Predictive Pipelined Decoding: A Compute-Latency Trade-off for Exact LLM Decoding. *TMLR* (2024).

[38] Jun Zhang, Jue Wang, Huan Li, Lidan Shou, Ke Chen, Gang Chen, and Sharad Mehrotra. 2024. Draft& Verify: Lossless Large Language Model Acceleration via Self-Speculative Decoding. In *ACL*. 11263–11282.

[39] Shigeng Zhang, Yinggang Li, Xuan Liu, Song Guo, Weiping Wang, Jianxin Wang, Bo Ding, and Di Wu. 2020. Towards Real-Time Cooperative Deep Inference over the Cloud and Edge End Devices. *IMWUT* 4, 2 (2020), 69:1–69:24.

[40] Susan Zhang, Stephen Roller, Naman Goyal, Mikel Artetxe, Moya Chen, Shuohui Chen, Christopher Dewan, Mona Diab, Xian Li, Xi Victoria Lin, et al. 2022. OPT: Open Pre-trained Transformer Language Models. arXiv:2205.01068 [cs.CL]

[41] Zhenyu Zhang, Ying Sheng, Tianyi Zhou, Tianlong Chen, Lianmin Zheng, et al. 2023. H2O: Heavy-Hitter Oracle for Efficient Generative Inference of Large Language Models. In *NIPS*. 34661–34710.

[42] Wayne Xin Zhao, Kun Zhou, Junyi Li, Tianyi Tang, Xiaolei Wang, Yupeng Hou, Yingqian Min, Beichen Zhang, Junjie Zhang, Zican Dong, et al. 2023. A Survey of Large Language Models. arXiv:2303.18223